Effect of Control Damping on Small-Signal Stability of Grid-Forming VSCs Considering Interaction Between Inner and Outer Loops

Jianing Liu, *Student Member, IEEE*, Yanghong Xia, *Member, IEEE*, Wei Wei, Qifan Feng, and Pengcheng Yang, *Member, IEEE*

***Abstract*—Strong coupling of conventional dual-loop control in *dq* frame makes stability analyses for grid-forming voltage-source converters (VSCs) inconvenient, hence the interaction between outer and inner loops is often omitted. However, this interaction plays an important role in system stability. To reduce the system orders, a decoupled inner-loop control method is proposed for grid-forming VSCs. This method has a similar damping adjustment ability to the dual-loop control, but can describe the inner-loop damping characteristic with only one parameter. With the help of this method, the effects of control damping and grid impedance on the system stability are revealed. First, the inner loop provides positive damping, which stabilizes the grid-forming VSCs. Second, the outer-loop droop control behaves as a negative damping characteristic which destabilizes the system, and larger droop coefficients can aggravate the negative damping and deteriorate the system stability. Third, the grid impedance can provide positive damping to the system, thus the grid-forming VSCs are prone to be stable under weak grid conditions. The analyses are verified by hardware-in-loop tests.**

***Index Terms*—Grid-forming voltage-source converter (VSC), impedance model, small-signal stability, system damping, weak grid.**

I. Introduction

A HIGH proportion of renewable energy access has led to the emergency and development of converter-dominant power grids [1], and consequently reduces the grid inertia and deteriorates the stability [2], [3]. Stability issues caused by interfaced voltage-source converters (VSCs) have attracted extensive attention in recent years [4], [5]. These grid-connected VSCs can be divided into grid-following VSCs and grid-forming VSCs according to their control strategies, and generally adopt different synchronization methods [6]. The grid-following VSCs approximately act as current sources and mainly use a phase-locked loop (PLL) to keep synchronization [7]. PLL-based VSCs are widely utilized in photovoltaic and wind-power generations [7], but they also raise serious stability issues, especially under weak grid conditions [8]. In contrast, the grid-forming VSCs nearly act as voltage sources, and they generally achieve synchronization through transient power transfer, which is similar to synchronous machines [9]. The strategies of grid-forming VSCs can achieve inertia improvement, voltage support, and particular enhancement of the stability when the VSCs are connected to weak grids [10]. Therefore, the grid-forming strategies are deemed as feasible measures to continuously improve the penetration of renewable energies [11].

The mission of a grid-connected grid-forming VSC is to generate certain active and reactive power according to the instantaneous amplitude and frequency difference between references and actual voltage at the point of common coupling (PCC), which can actively provide voltage and frequency support. Many strategies can be classified as grid-forming control besides classic droop control, such as droop control with additional low-pass filters [12], power-synchronization control [9], virtual synchronous generators [13], and synchronverter [14]. Most of these strategies mainly focus on the outer loop, and their foundation can be attributed to the droop control with additional inertia or damping terms [15]. As for the inner loop, the voltage and current dual-loop control based on proportional resonant (PR) controllers or proportional integral (PI) controllers is a typical and widely-used method since it is of intuitive consistency with grid-following strategies [16], [17], and this consistency is friendly to parameter tuning and stability analyses.

Stability analyses for grid-forming VSCs are often performed on the assumption that the outer loop and inner loop are decoupled, which means the inner loop can be ignored, and it is used not only in transient stability analyses [15], [18], but also in small-signal stability analyses [19], [20]. This assumption ignores the interaction between the control loops, that is, the outer-loop and inner-loop damping or inertia characteristics can influence each other. The interaction between control loops of VSCs is investigated in [21], and it points out that even a reasonable tuning method of inner-loop parameters can still cause the coupling of control loops. Furthermore, it is elaborated

Manuscript received 24 October 2023; revised 27 January 2024; accepted 12 March 2024. Date of publication 25 March 2024; date of current version 19 April 2024. This work was supported in part by the National Key R&D Program of China under Grant 2021YFB2401303, in part by the Key R&D Program of Zhejiang Province under Grant 2023C01126, and in part by the Science and Technology Project of State Grid Corporation of Zhejiang Province under Grant 5211DS230003. Recommended for publication by Associate Editor F. J. Azcondo. *(Corresponding author: Yanghong Xia.)*

The authors are with the College of Electrical Engineering, Zhejiang University, Hangzhou 310027, China (e-mail: ljn94@zju.edu.cn; royxiayh@zju.edu.cn; wwei@zju.edu.cn; 12110032@zju.edu.cn; ypc_196@zju.edu.cn).

Color versions of one or more figures in this article are available at https://doi.org/10.1109/TPEL.2024.3381148.

Digital Object Identifier 10.1109/TPEL.2024.3381148

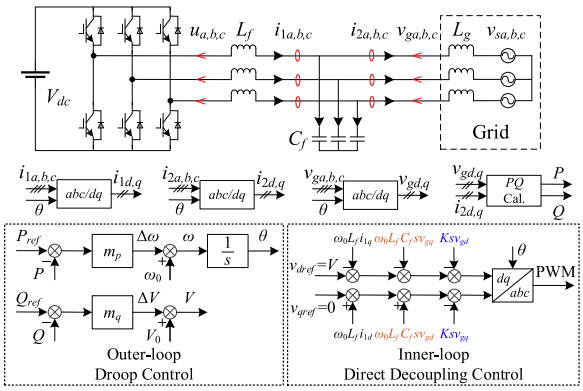

Fig. 1. Structure of the grid-forming VSC based on droop control and DDC.

in [22] that the coupling effect may happen under varying grid condition, which means the preset parameters cannot completely achieve the decoupling of control loops. To cope with the coupling effect between the control loops, a parameter tuning method based on eigenvalue parametric sensitivities is proposed in [23]. Although this method can improve the efficiency of the parameter tuning, it cannot intuitively describe or demonstrate the coupling relationship. In fact, state-space methods [23], [24] are not good methods for illustrating the interaction between control loops, since all factors are mixed, making it difficult to intuitively discuss the system model itself. This leads to a lack of in-depth understanding of the interactions between the control loops.

To better characterize the relationship between the control loops, an impedance circuit model of grid-forming converters is established in [25], and it visualizes the controller parameters of voltage and current dual-loop control as circuit elements to deepen the understanding of the interactions. However, this method does not reduce the complexity of the system, and the complicated high-order model makes it necessary to simplify some important factors. For example, the reactive-voltage droop is simplified as a virtual reactance in [25], and thus the effect of varying reactive droop coefficients cannot be directly reflected in the output admittance model. The high-order model of the system is mainly caused by *dq*-frame coupling, which is also the main reason that the inner-loop control is often omitted and some accuracy is sacrificed.

The essential function of inner voltage and current loops is to implement tracking control, while in this process, different types of control damping are introduced. Studying damping characteristics is an effective way to reveal the relationship between control loops, and it can also be used to study the relationship between inner and outer loops. To clearly describe the damping effect and the coupling relationship of inner and outer control, a simplified inner-loop control method named direct decoupling control (DDC) is proposed in this article. The DDC has a completely decoupled impedance model in *dq* frame, and it can describe the damping characteristic of the inner loop with only one parameter. Hence, the DDC is friendly to stability analyses and parameter tuning. The comparison between DDC and dual-loop control shows that it can be a representation of the inner-loop damping characteristic, and thus can guide the shaping of the inner loop. From the perspective of the damping effect, the relationship between outer and inner loops is revealed. That is, the inner-loop control is equivalent to an impedance with positive damping and it can totally reverse the negative damping effect of the outer-loop droop control. Furthermore, the single outer-loop model of grid-forming VSCs is an unstable model due to its negative damping effect. This suggests that the simplification of considering the inner-loop transfer function as unity gain may not be accurate. The influences of inner-loop and outer-loop parameters on system damping and stability are investigated in detail, and all analyses are verified by hardware-in-loop (HIL) tests.

The rest of this article is organized as follows. In Section II, the small-signal model of DCC-based VSC is established and compared with dual-loop control. In Section III, the negative damping effect of outer-loop droop control is revealed. In Section IV, the relationship between inner and outer loops is discussed and detailed stability analyses are performed. In Section V, the analyses are verified by HIL tests. Finally, Section VI concludes this article.

II. Modeling and Control of Grid-Forming VSCs Based On DDC

A. Modeling of Grid-Forming VSC Based on DDC

The structure of the grid-forming VSC is shown in Fig. 1. The VSC is filtered by an *LC* filter whose inductance and capacitance are L_f and C_f, respectively. The power grid is modeled by an ideal ac voltage source $v_{sa,b,c}$ in series with grid inductance L_g. The change of L_g can reflect different grid strengths. On the ac side, $u_{a,b,c}$ denotes the unfiltered voltages of the VSC. $i_{1\,a,b,c}$ denotes the currents flowing through L_f. $v_{ga,b,c}$ and $i_{2\,a,b,c}$ are the output voltages and currents at the PCC, respectively. The dc-link voltage is represented by a constant dc voltage source $V_{\rm dc}$. These symbols are used both in the time and frequency domain for simplicity. The model of the VSC connected to the weak grid in *dq* frame (after Laplace transformation) can be established as [26]

$$\begin{cases} sL_f i_{1d} = d_d V_{dc} - v_{gd} + \omega L_f i_{1q} \\ sL_f i_{1q} = d_q V_{dc} - v_{gq} - \omega L_f i_{1d} \\ sC_f v_{gd} = i_{1d} - i_{2d} + \omega C_f v_{gq} \\ sC_f v_{gq} = i_{1q} - i_{2q} - \omega C_f v_{gd} \\ sL_d i_{2d} = v_{gd} - v_{sd} + \omega L_g i_{2q} \\ sL_g i_{2q} = v_{gq} - v_{sq} - \omega L_g i_{2d} \end{cases} \tag{1}$$

where d_d and d_q are the duty ratio, and ω is the angular frequency. The outer loop consists of classical P–ω droop and Q–V droop, which is

$$\theta = \frac{\omega}{s} = \frac{1}{s}\left(m_p\left(P_{\rm ref} - P\right) + \omega_0\right) \tag{2}$$

$$V = m_q\left(Q_{\rm ref} - Q\right) + V_0 \tag{3}$$

where P and $P_{\rm ref}$ denote the active power and its reference value, while Q and $Q_{\rm ref}$ denote the reactive power and its reference value. m_p and m_q are the active power droop coefficient and

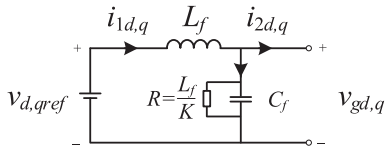

Fig. 2. Circuit model of the damping effect of DDC.

the reactive power droop coefficient, respectively. The voltage amplitude V and the angle θ are used for inner-loop control. V_0 and ω_0 denote the steady-state value of V and ω.

The inner loop of a grid-forming VSC is generally established on a synchronous dq frame, and one of its most important roles is to provide active damping to suppress the LC resonance. The conventional dual-loop inner loop cannot be completely decoupled in the dq frame, which means its impedance model contains off-diagonal elements. Consequently, the inner-loop model is a 2×2 matrix, which makes stability analyses much more complicated. In fact, as long as the decoupling term is added to the inner loop, the decoupling of the dq axes can be achieved. With an additional damping term, the inner loop can also actively suppress the LC resonance. The principle of the DDC is

$$\begin{cases} d_d = \frac{1}{V_{\rm dc}}\left(v_{d\rm ref} - \omega L_f i_{1q} - \omega L_f C_f s v_{gq} - K s v_{gd}\right) \\ d_q = \frac{1}{V_{\rm dc}}\left(v_{q\rm ref} + \omega L_f i_{1d} + \omega L_f C_f s v_{gd} - K s v_{gq}\right) \end{cases}. \quad (4)$$

In (4), $\omega L_f i_{1\,d,q}$ and $\omega L_f C_f s v_{gd,q}$ are the decoupling terms, and $K s v_{gq,d}$ is the damping term. K denotes the damping coefficient. Linearizing (1) and (4), the small-signal model of the DDC-based inner loop can be derived as

$$\begin{cases} \Delta v_{gd} = G_{\rm inner}\Delta v_{d\rm ref} - Z_{\rm inner}\Delta i_{2d} \\ \Delta v_{gq} = G_{\rm inner}\Delta v_{q\rm ref} - Z_{\rm inner}\Delta i_{2q} \end{cases} \quad (5)$$

where

$$G_{\rm inner} = \frac{1}{L_f C_f s^2 + K s + 1} \quad (6)$$

$$Z_{\rm inner} = \frac{L_f s}{L_f C_f s^2 + K s + 1}. \quad (7)$$

The small-signal variables are denoted by Δ. It is shown that not only the closed-loop transfer function, but also the impedance model can be regarded as a single-input single-output system, which is very friendly to stable analyses. According to the small-signal model, the damping term introduces capacitance-voltage differential feedback, which can be regarded as a parallel resistor on the filter capacitor and the resistance is L_f / K. The circuit model is shown in Fig. 2. It can be inferred that if K is very large, the filter capacitor will be bypassed, while if K is very small, the parallel resistor will be equivalent to an open-circuit, which means the system lacks damping. The coefficient K itself can reflect the whole damping characteristic of the inner loop, and it should be properly designed.

The inner-loop control based on the DDC still has high-frequency noise suppression ability, although the differential is utilized. Assuming that the noise perturbance N is introduced in the d-axis voltage, i.e.,

$$v_{gd\_N} = v_{gd} + N. \quad (8)$$

Then the small-signal model becomes

$$\begin{cases} \Delta v_{gd} = G_{\rm inner}\Delta v_{d\rm ref} - Z_{\rm inner}\Delta i_{2d} - \frac{Ks}{L_f C_f s^2 + Ks + 1}\Delta N \\ \Delta v_{gq} = G_{\rm inner}\Delta v_{q\rm ref} - Z_{\rm inner}\Delta i_{2q} + \frac{\omega L_f C_f s}{L_f C_f s^2 + Ks + 1}\Delta N \end{cases}. \quad (9)$$

According to the transfer function from the noise N to the PCC voltage $v_{gd,q}$, the noise signals are not amplified and can be suppressed at high frequencies. It is the same when the noise is introduced in the q-axis.

The main purpose of the inner loop is to track the voltage reference so that the VSC can generate expected active and reactive power. The voltage-following function of the DDC is verified based on a scenario in which the grid-forming VSC is connected to a resistive load. As a result, voltages under different K are shown in Fig. 3, where a step voltage reference signal is performed. It is shown that the DDC can achieve voltage tracking, and with different K, the system damping characteristic is changed.

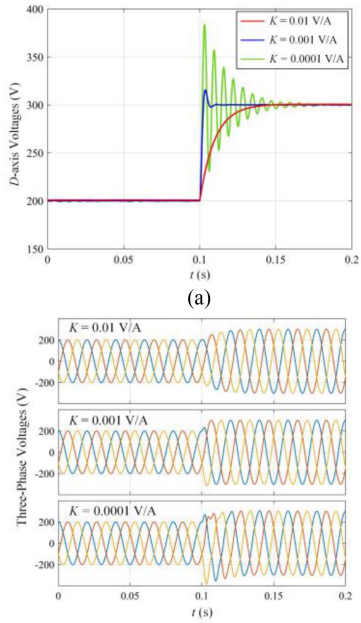

Fig. 3. Voltages when K changes from 1×10^{-2} V/A to 1×10^{-4} V/A. (a) D-axis voltages. (b) Three-phase voltages.

B. Comparison With Dual-Loop Control

Fig. 4 shows the widely-used dual-loop control and its circuit model, where current and voltage feedforwards are applied. F_i and F_v are the current and voltage feedforward coefficients, respectively. In [25], it is pointed out that the current loop can be regarded as an equivalent virtual impedance Z_1 in series with the filter inductance L_f, and the voltage loop is equivalent to an additional virtual impedance Z_2 in parallel with the filter capacitance C_f. Another impedance Z_3 is affected by F_i and F_v.

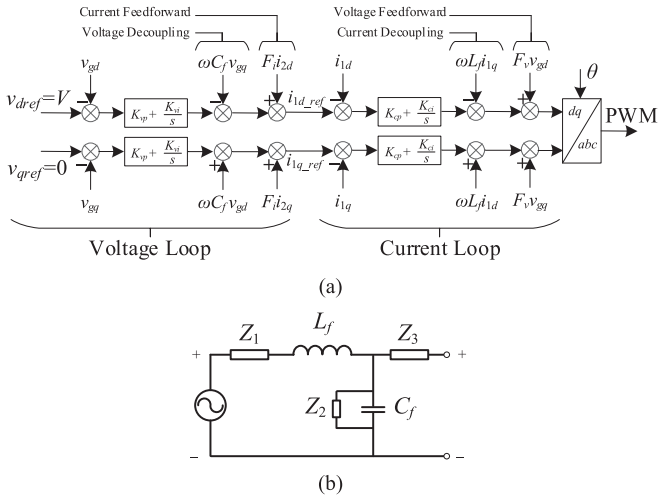

Fig. 4. Voltage and current dual-loop control. (a) Control strategy. (b) Circuit model.

The current and voltage feedforward can help to eliminate the disturbance of the grid, but they also may introduce negative damping or even cause instability. The damping characteristic of the dual-loop control is related to three virtual impedances and six parameters, and it is more difficult to describe compared with the DDC. Note that damping effects brought by Z_1, Z_2, and Z_3 are inherently introduced by the control for reference tracking and feedforward, and they are not all necessary to suppress the *LC* resonance.

Linearize the control loop shown in Fig. 4 and submit it into linearized (1), the inner-loop model based on the dual-loop control can be derived as

$$\begin{bmatrix}\Delta v_{gd}\\ \Delta v_{gq}\end{bmatrix}=\begin{bmatrix}G_{dd} & G_{dq}\\ G_{qd} & G_{qq}\end{bmatrix}\begin{bmatrix}\Delta v_{\mathrm{dref}}\\ \Delta v_{\mathrm{qref}}\end{bmatrix}-\begin{bmatrix}Z_{dd} & Z_{dq}\\ Z_{qd} & Z_{qq}\end{bmatrix}\begin{bmatrix}\Delta i_{2d}\\ \Delta i_{2q}\end{bmatrix} \tag{10}$$

where

$$G_{dd}=G_{qq}=\frac{\left(\left(C_f s+\mathrm{PI}_v\right)\mathrm{PI}_c+C_f L_f s^2-F_v+1\right)\mathrm{PI}_c\mathrm{PI}_v}{D\left(s\right)} \tag{11}$$

$$G_{dq}=-G_{qd}=\frac{C_f L_f \mathrm{PI}_c \mathrm{PI}_v \omega s}{D\left(s\right)} \tag{12}$$

$$Z_{dd}=Z_{qq}=\frac{\left(C_f L_f s^2+\mathrm{PI}_c\left(\mathrm{PI}_v+C_f s\right)-F_v+1\right)\left(sL_f-\mathrm{PI}_c\left(F_i-1\right)\right)}{D\left(s\right)} \tag{13}$$

$$Z_{dq}=-Z_{qd}=\frac{sC_f L_f \omega\left(sL_f-\mathrm{PI}_c\left(F_i-1\right)\right)}{D\left(s\right)} \tag{14}$$

$$\begin{aligned}D\left(s\right)=&\left(C_f s+\mathrm{PI}_v\right)^2\mathrm{PI}_c^2+\left(2\left(C_f s+\mathrm{PI}_v\right)\right)\left(C_f L_f s^2\right.\\&\left.-F_v+1\right)\mathrm{PI}_c+s^2L_f^2\left(s^2+\omega^2\right)C_f^2-2s^2L_f\\&\left(F_v-1\right)C_f+\left(F_v-1\right)^2.\end{aligned} \tag{15}$$

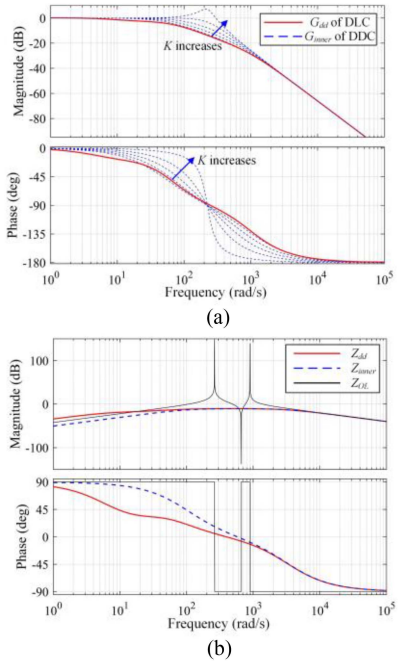

Fig. 5. Bode diagrams of DLC and DDC. (a) Closed-loop transfer function. (b) Impedance model comparison with open-loop impedance.

$\mathrm{PI}_v=K_{vp}+K_{vi}/s$, and $\mathrm{PI}_c=K_{cp}+K_{ci}/s$. They are the PI controllers of the voltage loop and current loop, respectively. Bode diagrams of the two inner controllers are shown in Fig. 5. The coupling terms of the dual-loop control are not shown for simplicity.

For the closed-loop transfer function, the Bode diagrams of G_{dd} and G_{inner} with different K are shown in Fig. 5(a), and the two control methods show a high consistency: First, the inner loop under both methods exhibits a low-pass characteristic, hence high-frequency noise comes from the outer loop can be suppressed. Second, the proposed DDC can mimic the damping properties of the dual-loop control by adjusting K, thus they have similar damping adjustment abilities. Furthermore, the cutoff frequency of dual-loop control is affected by the bandwidth of the current loop and the voltage loop, but it is mainly determined by the *LC* filter for resonance suppression. The cutoff frequency of the DDC is also determined by the parameters of *LC*, hence the two control methods have similar bandwidth. For the impedance model, Fig. 5(b) shows the Bode diagrams of Z_{OL} of the open-loop circuit, Z_{dd} of the dual-loop control, and Z_{inner} of DDC with a particular K which makes the damping characteristic of DDC closest to the dual-loop control. From the bode diagrams, the suppression of the inner loop on the *LC* resonance is clearly presented.

In conclusion, the DDC shows very similar damping adjustment characteristics to the dual-loop control. The damping coefficient K introduces a parallel resistor to the filter capacitor, and can suppress the *LC* resonance as the same as the dual-loop control. In other words, the DDC can represent the damping effect of the dual-loop control and can help to reveal the effect of control damping on system stability.

III. Damping Analysis of Outer-Loop Droop Control

In many studies, the inner loop of a grid-forming VSC is simplified to a unity gain during stability analyses, provided that the inner loop and the outer loop are decoupled in response time. The main reason for this simplification is that the inner-loop dual-loop control is with coupled terms, and hence with a high-order model. However, the inner loop as well as its coupling with the outer loop is inevitable because the widely used droop control cannot bring any damping to the system, which means the simplification will introduce some errors. The damping deficiency will be shown in this section.

When the influence of the inner loop and the filter is removed, the grid-forming VSC can be regarded as a controlled voltage source whose voltage amplitude and phase angle are given by the outer-loop droop control. The linearized small-signal model of the outer-loop droop control can be derived as

$$\Delta\theta = \frac{1}{s}\left(m_p\left(0-\Delta P\right)\right) \tag{16}$$

$$\Delta V = m_q\left(0-\Delta Q\right). \tag{17}$$

ΔP and ΔQ denote the small-signal active and reactive power respectively, i.e.,

$$\Delta P = 1.5\left(V_{gd}^*\Delta i_{2d} + I_{2d}^*\Delta v_{gd} + V_{gq}^*\Delta i_{2q} + I_{2q}^*\Delta v_{gq}\right) \tag{18}$$

$$\Delta Q = 1.5\left(V_{gq}^*\Delta i_{2d} + I_{2d}^*\Delta v_{gq} - V_{gd}^*\Delta i_{2q} - I_{2q}^*\Delta v_{gd}\right). \tag{19}$$

The superscript $*$ represents the steady-state value of the variables. Combining (16)–(19), the small-signal PCC voltage in dq frame can be expressed as

$$\begin{bmatrix}\Delta v_{gd}\\ \Delta v_{gq}\end{bmatrix} = \begin{bmatrix}\Delta V\\ V_0\Delta\theta\end{bmatrix} = \boldsymbol{G_V}\begin{bmatrix}\Delta i_{2d}\\ \Delta i_{2q}\end{bmatrix} + \boldsymbol{G_I}\begin{bmatrix}\Delta v_{gd}\\ \Delta v_{gq}\end{bmatrix} \tag{20}$$

where

$$\boldsymbol{G_V} = \begin{bmatrix}-1.5m_qV_{gq}^* & 1.5m_qV_{gd}^*\\ -1.5V_0m_pV_{gd}^*/s & -1.5V_0m_pV_{gq}^*/s\end{bmatrix} \tag{21}$$

$$\boldsymbol{G_I} = \begin{bmatrix}1.5m_qI_{2q}^* & -1.5m_qI_{2d}^*\\ -1.5V_0m_pI_{2d}^*/s & -1.5V_0m_pI_{2q}^*/s\end{bmatrix}. \tag{22}$$

The impedance model can be derived as

$$\boldsymbol{Z_{outer}} = -(\boldsymbol{I}-\boldsymbol{G_I})^{-1}\boldsymbol{G_V} \tag{23}$$

where $\boldsymbol{I}$ denotes the identity matrix. For simplicity, assume that $V_{gq}^* = 0$, and $I_{2q}^* = 0$, which is a common condition where the VSC works with a unity power factor and does not generate reactive power. Then, the impedance model is simplified as

$$\boldsymbol{Z_{outer}} = \begin{bmatrix}\frac{9m_qI_{2d}^*V_{gd}^*m_pV_0}{9I_{2d}^{*2}V_0m_pm_q-4s} & \frac{6m_qV_{gd}^*s}{9I_{2d}^{*2}V_0m_pm_q-4s}\\ -\frac{6V_0V_{gd}^*m_p}{9I_{2d}^{*2}V_0m_pm_q-4s} & \frac{9m_qI_{2d}^*V_{gd}^*m_pV_0}{9I_{2d}^{*2}V_0m_pm_q-4s}\end{bmatrix}. \tag{24}$$

Temporarily, a resistor R_g is considered in the grid impedance model to represent the damping effect of the system, thus the grid impedance model can be derived as

$$\boldsymbol{Z_g} = \begin{bmatrix}L_gs+R_g & -\omega L_g\\ \omega L_g & L_gs+R_g\end{bmatrix}. \tag{25}$$

Then, the system stability can be analyzed by the root of the closed-loop characteristic equation, i.e., $\det(\boldsymbol{Z_{outer}}+\boldsymbol{Z_g})=0$, and it can be derived as

$$d_3s^3 + d_2s^2 + d_1s^1 + d_0 = 0 \tag{26}$$

where

$$\begin{cases} d_3 = 4L_g^2\\ d_2 = -9I_{2d}^{*2}L_g^2V_0m_pm_q + 8L_gR_g\\ d_1 = 4L_g^2\omega^2 + \left(-18I_{2d}^{*2}R_gV_0m_p + 6V_{gd}^*\omega\right)m_qL_g + 4R_g^2\\ d_0 = 9V_0m_pm_q\left(V_{gd}^{*2} - I_{2d}^{*2}\left(\omega^2L_g^2 + R_g^2\right)\right)\\ \qquad +6\omega L_gV_0V_{gd}^*m_p \end{cases}. \tag{27}$$

For a third-order system, the coefficient d_2 can reflect the damping of the system to some extent. For example, assume that a third-order system consists of three one-order systems, and its characteristic equation is derived as

$$(s+a)(s+b)(s+c) = 0 \tag{28}$$

where a, b, and c are real numbers. Then $d_2 = a+b+c$, which means the smaller d_2, the smaller one of a, b, and c, and the smaller damping of one of the one-order systems. If $d_2<0$, either a, b, or c must be negative, and the system will be unstable due to the negative damping. This phenomenon also exists in the case that the third-order system is made up of a one-order system and a second-order system, i.e., the characteristic equation becomes

$$(s+a)(s+b+jc)(s+b-jc) = 0. \tag{29}$$

Then, $d_2 = a+2b$, and d_2 can also reflect the system damping. This relationship is intuitive on the condition that the system is simple and with a low-order model.

Therefore, as for (27), if $R_g=0$, then $d_2<0$, the system cannot be stable. With the incremental R_g, two characteristic roots move to the left in the s-plane as shown in Fig. 6(a), which means the damping of the system is enhanced. However, the damping is introduced and enhanced by the grid impedance rather than the outer-loop droop control. It can be seen from the expression of d_2 that the increased droop coefficients will behave as the same effect as the negative grid resistance, which means it will introduce negative damping to the system. The trajectory of the poles with incremental m_p is shown in Fig. 6(b), which can verify the negative damping effect of the outer-loop droop control.

To verify the negative damping characteristic of the outer-loop droop control, a simulation model shown in Fig. 7 is established based on MATLAB/Simulink. The grid-forming VSC is modeled by a three-phase voltage source whose voltage is directly regulated by the outer loop, and thus the influence of the inner loop, as well as the LC filter, is ignored.

Fig. 8(a) shows the active power P of the controlled voltage source when R_g decreases. It is shown that with the R_g decreasing, the damping of the system is accordingly decreased, and the dynamic response time becomes longer, or even an oscillation happens. Fig. 8(b) shows the active power when m_p increases, and the trend of system damping change is consistent with the analyses, that is, the damping of the system is decreased as m_p increases until the system becomes unstable.

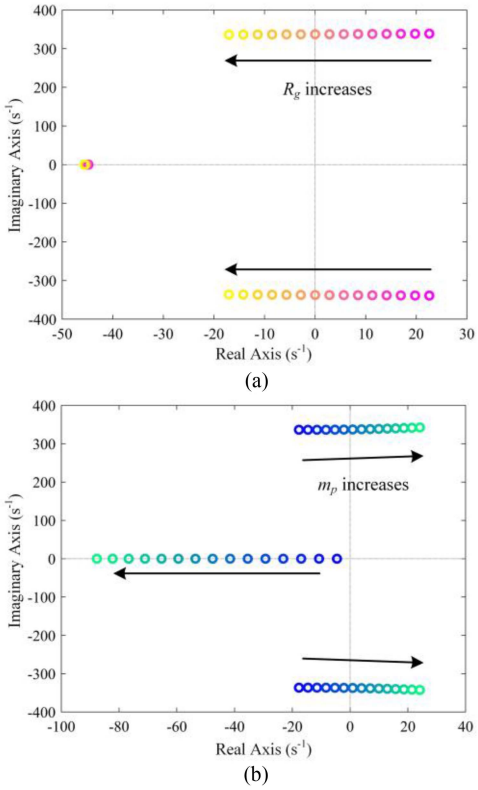

Fig. 6. Locus of the characteristic equation zeros. (a) R_g increases from 0 to 0.04 Ω. (b) m_p increases from 1×10^{-5} to 2×10^{-3} rad/s/W.

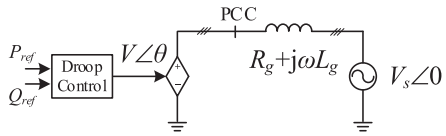

Fig. 7. Controlled voltage source model of the grid-forming VSC.

In conclusion, the outer-loop droop control will bring a negative damping effect to the system. The system under droop control needs inner-loop control to enhance the system damping. Furthermore, if the inner-loop control is omitted, i.e., simplified as a unity gain, the critical damping effect will be removed, hence this simplification is imprecise for small-signal stability analyses.

IV. Effect of Control Damping on Small-Signal Stability of Grid-Forming VSC

In this section, the influence of critical parameters such as droop coefficients, damping coefficient, and grid impedance on the small-signal stability will be studied. The advantage that the DDC can facilitate stability analyses by virtue of its completely decoupled characteristic will be presented.

When the outer loop and the inner loop are both taken into consideration, there will be a small phase angle disturbance between the system and the controller *dq* frames, which is introduced by the outer-loop *P*-ω droop. To distinguish them, the system *dq* frame is represented by the superscript "*s*," and

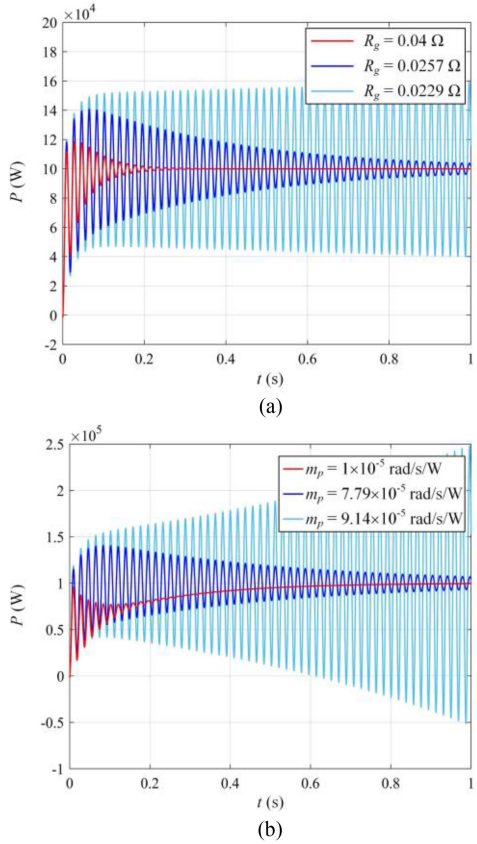

Fig. 8. Active power output when only considering the droop control. (a) Changing R_g. (b) Changing m_p.

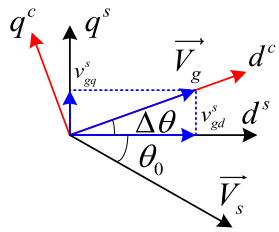

Fig. 9. Relationship of the two *dq* frames.

the controller *dq* frame is represented by the superscript "*c*." The relationship between the two frames is expressed as (30), and as an example, the PCC voltage in the two *dq* frames is shown in Fig. 9

$$\begin{cases} x_d^c = x_d^s cos\Delta\theta + x_q^s \sin\Delta\theta \\ x_q^c = x_q^s cos\Delta\theta - x_d^s \sin\Delta\theta \end{cases}. \tag{30}$$

Accordingly, the small-signal model of the VSC can be derived as

$$\begin{cases} sL_f\Delta i_{1d}^s = \Delta d_d^s V_{\rm dc} - \Delta v_{gd}^s + \omega L_f \Delta i_{1q}^s \\ sL_f\Delta i_{1q}^s = \Delta d_q^s V_{\rm dc} - \Delta v_{gq}^s - \omega L_f \Delta i_{1d}^s \\ sC_f\Delta v_{gd}^s = \Delta i_{1d}^s - \Delta i_{2d}^s + \omega C_f \Delta v_{gq}^s \\ sC_f\Delta v_{gq}^s = \Delta i_{1q}^s - \Delta i_{2q}^s - \omega C_f \Delta v_{gd}^s \end{cases}. \tag{31}$$

The small-signal model of the DDC in the controller *dq* frame is expressed as

$$\begin{cases}\Delta d_d^c = \frac{1}{V_{\rm dc}}\left(\Delta v_{d\rm ref} - \omega L_f \Delta i_{1q}^c - \omega L_f C_f s \Delta v_{gq}^c - Ks\Delta v_{gd}^c\right)\\ \Delta d_q^c = \frac{1}{V_{\rm dc}}\left(\Delta v_{q\rm ref} + \omega L_f \Delta i_{1d}^c + \omega L_f C_f s \Delta v_{gd}^c - Ks\Delta v_{gq}^c\right)\end{cases} \tag{32}$$

where

$$\begin{cases}\Delta v_{d\rm ref} = \Delta V\\ \Delta v_{q\rm ref} = V_0 \Delta\theta\end{cases}. \tag{33}$$

Convert the variables to the system *dq* frame, and then submit (32) into (31), we get

$$\begin{bmatrix}\Delta v_{gd}^s\\ \Delta v_{gq}^s\end{bmatrix} = G_{\rm inner}\begin{bmatrix}\Delta v_{d\rm ref}\\ \Delta v_{q\rm ref}\end{bmatrix} - Z_{\rm inner}\begin{bmatrix}\Delta i_{2d}^s\\ \Delta i_{2q}^s\end{bmatrix} + \boldsymbol{G_\theta}\Delta\theta \tag{34}$$

where

$$\boldsymbol{G_\theta} = \begin{bmatrix}\frac{\left(\omega C_f L_f V_{gd}^* - KV_{gq}^*\right)s + \omega L_f I_{1d}^* - D_q^* V_{\rm dc}}{L_f C_f s^2 + Ks + 1}\\ \frac{\left(\omega C_f L_f V_{gq}^* + KV_{gd}^*\right)s + \omega L_f I_{1q}^* + D_d^* V_{\rm dc}}{L_f C_f s^2 + Ks + 1}\end{bmatrix}. \tag{35}$$

$\boldsymbol{G}_\theta$ is the transfer function matrix from $\Delta\theta$ to $\Delta v_{gd,q}$, and it can be regarded as a filter of phase angle disturbance. Each element of $\boldsymbol{G}_\theta$ includes $G_{\rm inner}$ with different zero points, which means the inner-loop control is the foundation of elimination of phase angle disturbance, and hence the damping coefficient K also has an important influence on the phase angle disturbance elimination. Submit (18) and (19) into (33), it can be derived as

$$\begin{bmatrix}\Delta v_{d\rm ref}\\ \Delta v_{q\rm ref}\end{bmatrix} = \boldsymbol{G_V}\begin{bmatrix}\Delta i_{2d}^s\\ \Delta i_{2q}^s\end{bmatrix} + \boldsymbol{G_I}\begin{bmatrix}\Delta v_{gd}^s\\ \Delta v_{gq}^s\end{bmatrix} \tag{36}$$

$$\Delta\theta = \boldsymbol{V_{gdq}}\begin{bmatrix}\Delta i_{2d}^s\\ \Delta i_{2q}^s\end{bmatrix} + \boldsymbol{I_{2dq}}\begin{bmatrix}\Delta v_{gd}^s\\ \Delta v_{gq}^s\end{bmatrix} \tag{37}$$

where

$$\boldsymbol{V_{gdq}} = \begin{bmatrix}-\frac{1.5m_p V_{gd}^*}{s} & -\frac{1.5m_p V_{gq}^*}{s}\end{bmatrix} \tag{38}$$

$$\boldsymbol{I_{2dq}} = \begin{bmatrix}-\frac{1.5m_p I_{2d}^*}{s} & -\frac{1.5m_p I_{2q}^*}{s}\end{bmatrix}. \tag{39}$$

Submitting (36) and (37) into (34), the impedance model of the VSC can be derived as

$$\begin{aligned}\boldsymbol{Z}_{\rm VSC} = &-\left(\boldsymbol{I} - G_{\rm inner}\boldsymbol{G_I} - \boldsymbol{G_\theta I_{2dq}}\right)^{-1}\left(G_{\rm inner}\boldsymbol{G_V}\right.\\ &\left.-Z_{\rm inner}\boldsymbol{I} + \boldsymbol{G_\theta V_{gdq}}\right).\end{aligned} \tag{40}$$

A. Discussion About the Impedance Model

Comparing the inner-loop impedance $Z_{\rm inner}$, the outer-loop impedance $\boldsymbol{Z}_{\rm outer}$, and the complete impedance $\boldsymbol{Z}_{\rm VSC}$, some conclusions can be made. If the phase angle disturbance is not taken into consideration ($\boldsymbol{G}_\theta = \boldsymbol{0}$), and if the power disturbance caused by PCC voltage disturbance is ignored ($\boldsymbol{G_I}[\Delta v_{gd}^s \quad \Delta v_{gq}^s]^{\rm T} = 0$), which is a reasonable simplification utilized in [25], then it can be derived that

$$\boldsymbol{Z}_{\rm VSC} = G_{\rm inner}\boldsymbol{Z}_{\rm outer} - Z_{\rm inner}\boldsymbol{I}. \tag{41}$$

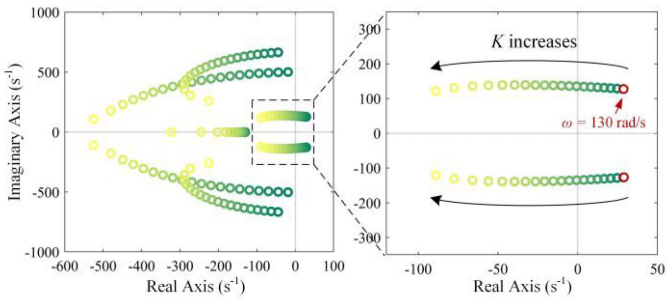

Fig. 10. Root locus when K changes from 0.002 to 0.02 V/A.

Accordingly, $Z_{\rm inner}$ can be deemed as an opposite impedance to $\boldsymbol{Z}_{\rm outer}$, and they are connected in series. The negative damping effect of $\boldsymbol{Z}_{\rm outer}$ has been revealed in Section II, therefore the inner lo control can be regarded as a kind of positive damping added to the outer loop, and it is essential to stabilize the system.

On the other hand, if $G_{\rm inner} = 1 / (L_f C_f s^2 + Ks + 1)$ is deemed as a complex gain whose amplitude is always less than 1, elements of $G_{\rm inner}\boldsymbol{Z}_{\rm outer}$ may have a negative real part with a smaller absolute value than that of $\boldsymbol{Z}_{\rm outer}$, which means $G_{\rm inner}$ can weaken the negative damping effect of the outer-loop control.

B. Detailed Stability Analyses

Stability analyses in this part are based on (40), which means all system and control elements are taken into consideration. Based on the impedance models, the system stability can be analyzed by the root locus of the characteristic equation, that is

$$\det\left(\boldsymbol{Z}_{\rm VSC} + \boldsymbol{Z_g}\right) = 0. \tag{42}$$

The damping effect of the inner loop is first studied, and in the following parts, the grid resistance is not considered, i.e., $R_g = 0$. Fig. 10 shows the root locus when K changes from 0.002 to 0.02 V/A. When $K = 0.002$ V/A, the system is unstable with negative damping and the oscillation frequency is 130 rad/s, while when $K = 0.02$ V/A, the system is stable with proper damping. The locus of the dominant poles illustrates that the inner-loop control provides sufficient damping to overcome the negative damping effect of the outer-loop control, and the system damping is increased as the inner-loop damping increases. The rigorous root locus analysis is consistent with the intuitive analysis of the impedance model, proving that the inner-loop damping plays a significant role in stabilizing the system.

Then, the influence of the grid impedance on system stability is studied. Fig. 11 shows the root locus of the system when L_g changes from 0.05 to 1 mH. From the dominant poles, it can be inferred that with the incremental L_g, the system is better damped, which means the weaker grid can introduce a stronger damping effect.

The negative damping effect of the outer-loop droop control can be studied in the same way. Fig. 12 shows the dominant poles of the system when m_p changes from 0.0003 to 0.003 rad/s/W. It can be seen that with the incremental P–ω droop coefficient, the damping of the system is decreased, and

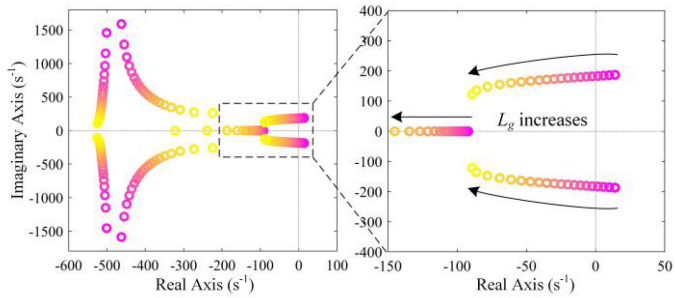

Fig. 11. Root locus when L_g changes from 0.05 to 1 mH.

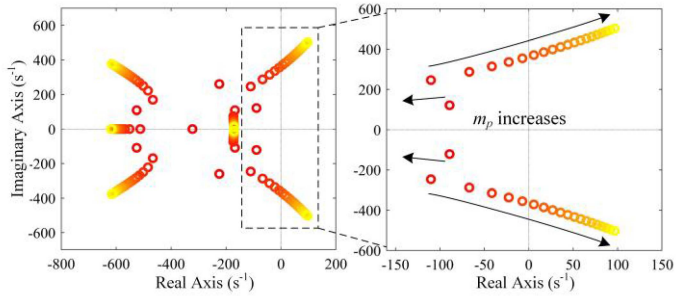

Fig. 12. Root locus when m_p changes from 0.0003 to 0.003 rad/s/W.

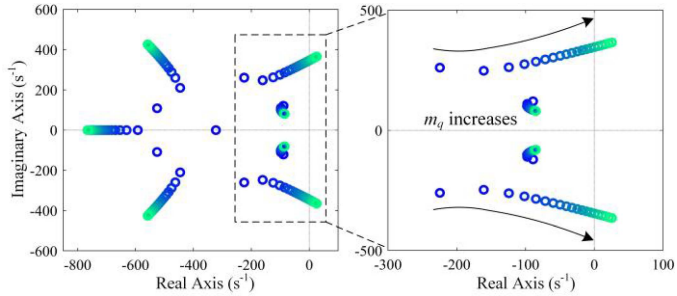

Fig. 13. Root locus when m_q changes from 0.002 to 0.007 V/var.

the stability is weakened. Fig. 13 shows the dominant poles when m_q changes from 0.002 to 0.007 V/var. It can be seen that with the incremental Q–V droop coefficient, the damping of the system is decreased. The root locus analyses indicate that the negative damping effect of the outer loop is aggravated as the droop coefficient increases, which means the analysis results are consistent with the results of Section II when both inner and outer loops are considered.

With the help of the DDC, the damping feature of the inner loop control is extracted. The inner-loop model is completely decoupled in dq frame, which can avoid the inconvenience of stability analyses caused by high-order models, and consequently can make the interaction between the inner loop and the outer loop more comprehensible. The outer-loop droop control introduces negative damping to the system, thus it is harmful to the stability. While the inner-loop control can provide positive damping, hence it stabilizes the system. The inner loop is important for system stability, which means it cannot be

Fig. 14. HIL test platform.

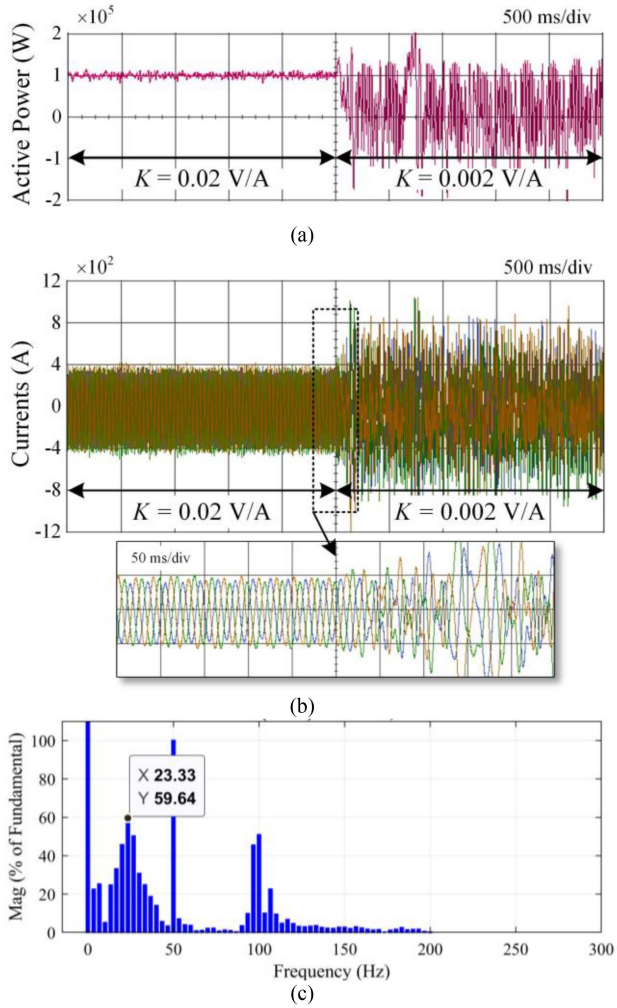

Fig. 15. Waveforms when K decreases. (a) Active power. (b) Three-phase currents. (c) Spectral analysis of the a-phase current.

simply ignored. Moreover, the function of the inner loop can be supplemented and summarized as follows.

1) It achieves voltage tracking, and makes the VSC output certain active and reactive power.
2) It suppresses the LC resonance caused by the filter.
3) It provides damping to the outer-loop droop control, which is essential for the system to keep stable.

V. HIL Verification

In this section, analysis results of Section III are tested utilizing RTLAB real-time emulator and TMS320F28335 DSP. The test platform is presented in Fig. 14, where the main

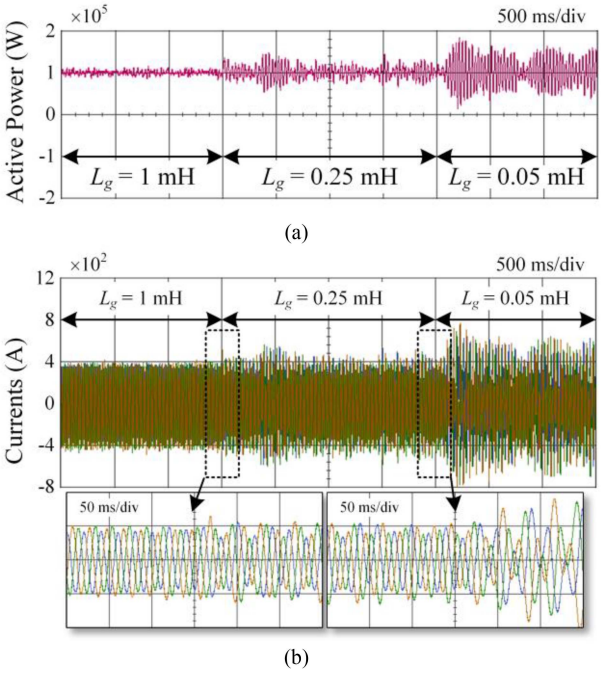

Fig. 16. Waveforms when L_g decreases. (a) Active power. (b) Three-phase currents.

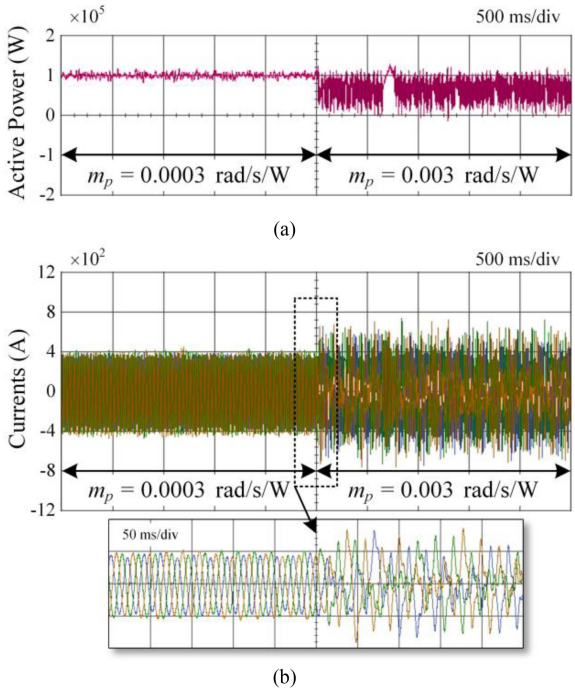

Fig. 17. Waveforms when m_p increases. (a) Active power. (b) Three-phase currents.

circuit of Fig. 1 is simulated in the RTLAB, and the control strategy is executed by the DSP. In the DSP control algorithm, the differentiation terms in (4) are implemented by difference operations, that is, $dv_{gd,q}(t)/dt \approx (v_{gd,q}(t)\text{-}v_{gd,q}(t\text{-}T_s))/T_s$, where T_s is the control cycle. Unless otherwise specified, parameters listed in Table I are used.

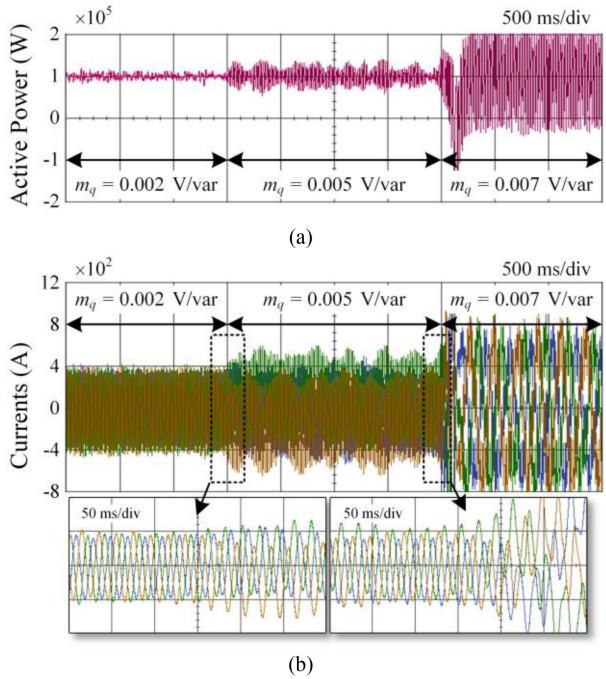

Fig. 18. Waveforms when m_q increases. (a) Active power. (b) Three-phase currents.

TABLE I
MAIN SYSTEM PARAMETERS

Parameters	Value
L_f, C_f	5 mH, 4 mF
L_g	1 mH
P_{ref}, Q_{ref}	100 kW, 0 var
V_0, ω_0	311 V, 100 π rad/s
K	0.02 V/A
m_p, m_q	0.0003 rad/s/W, 0.002 V/var
T_s	5×10^{-5} s

First, the effect of the damping coefficient K and the grid impedance L_g on the system stability is verified. The active power and the three-phase currents when K changes from 0.02 to 0.002 V/A are shown in Fig. 15. As predicted by the theoretical analyses, the system becomes unstable when the inner-loop damping is insufficient. Based on the fast fourier transform (FFT), the spectral analysis of the a-phase current when K = 0.002 V/A is shown in Fig. 15(c) and the oscillation with a frequency of 20.33 Hz is the most prominent component. This result is also consistent with Fig. 10, and the correctness of the model is verified.

Fig. 16 shows the active power and three-phase currents when L_g changes from 1 to 0.25 mH and 0.05 mH. When L_g = 1 mH, the system is stable, and the VSC generates the expected power, which verifies the effectiveness of the DDC. When L_g decreases to 0.25 mH, the system damping is lower and the stability is weakened. When L_g decreases to 0.05 mH, the system becomes unstable as predicted by Fig. 11. This phenomenon illustrates that the grid-forming VSC that behaves as a voltage source is easier to be stable under a weak grid, thus it is more suitable for a converter-dominated grid.

Then, the effect of the droop coefficients m_p and m_q on the system stability is tested. Fig. 17 shows the active power and the currents of the VSC when m_p changes from 0.0003 to 0.003 rad/s/W. Due to its negative damping effect, the system becomes unstable when m_p is unreasonably large. These test results are consistent with the theoretical analyses presented in Fig. 12. Similar tests are performed for changing m_q, and the results are shown in Fig. 18. When m_q changes from 0.002 to 0.005 V/var, the system stability deteriorates, and finally, the system becomes unstable when m_q is set to 0.007 V/var. These test results are successfully predicted by the analyses presented in Fig. 13, where the system dominant poles move to the right as m_q increases, and consequently, the stability is continuously getting worse.

VI. Conclusion

This article presents a decoupled inner-loop control method for grid-forming VSCs. This method can achieve the same function as the voltage and current dual-loop control and has a similar damping adjustment ability. More importantly, it can simplify the characterization of the inner-loop control damping, which is friendly to stability analyses and parameter tuning. With the help of this method, the controller damping effect of grid-forming VSCs is clearly revealed. On the one hand, the inner-loop control can be regarded as a complex gain that can weaken the negative damping effect of the outer-loop droop control. On the other hand, the inner loop impedance with positive damping can completely reverse the negative damping effect of the outer loop. Therefore, inner-loop control is essential for stabilizing the system. Furthermore, the larger droop coefficients, the stronger outer-loop negative damping, and grid-forming VSCs are easier to be stable under weaker grid conditions since the grid impedance also can provide positive system damping.

References

[1] N. Hatziargyriou et al., "Definition and classification of power system stability – revisited & extended," *IEEE Trans. Power Syst.*, vol. 36, no. 4, pp. 3271–3281, Jul. 2021.

[2] Y. Chi et al., "Overview of mechanism and mitigation measures on multi-frequency oscillation caused by large-scale integration of wind power," *CSEE J. Power Energy Syst.*, vol. 5, no. 4, pp. 433–443, Dec. 2019.

[3] F. Milano, F. Dörfler, G. Hug, D. J. Hill, and G. Verbič, "Foundations and challenges of low-inertia systems," in *Proc. Power Syst. Comput. Conf.*, 2018, pp. 1–25.

[4] X. Wang and F. Blaabjerg, "Harmonic stability in power electronic-based power systems: Concept, modeling, and analysis," *IEEE Trans. Smart Grid*, vol. 10, no. 3, pp. 2858–2870, May 2019.

[5] J. Shair, X. Xie, L. Wang, W. Liu, J. He, and H. Liu, "Overview of emerging subsynchronous oscillations in practical wind power systems," *Renew. Sustain. Energy Rev.*, vol. 99, pp. 159–168, Jan. 2019.

[6] J. Rocabert, A. Luna, F. Blaabjerg, and P. Rodríguez, "Control of power converters in ac microgrids," *IEEE Trans. Power Electron.*, vol. 27, no. 11, pp. 4734–4749, Nov. 2012.

[7] S. Golestan and J. M. Guerrero, "Conventional synchronous reference frame phase-locked loop is an adaptive complex filter," *IEEE Trans. Ind. Electron.*, vol. 62, no. 3, pp. 1679–1682, Mar. 2015.

[8] S. Golestan, J. M. Guerrero, and J. C. Vasquez, "Three-phase PLLs: A review of recent advances," *IEEE Trans. Power Electron.*, vol. 32, no. 3, pp. 1894–1907, Mar. 2017.

[9] B. Wen, D. Boroyevich, R. Burgos, P. Mattavelli, and Z. Shen, "Analysis of D-Q small-signal impedance of grid-tied inverters," *IEEE Trans. Power Electron.*, vol. 31, no. 1, pp. 675–687, Jan. 2016.

[10] L. Zhang, L. Harnefors, and H.-P. Nee, "Power-synchronization control of grid-connected voltage-source converters," *IEEE Trans. Power Syst.*, vol. 25, no. 2, pp. 809–820, May 2010.

[11] R. Rosso, X. Wang, M. Liserre, X. Lu, and S. Engelken, "Grid-forming converters: Control approaches, grid-synchronization, and future trends—A review," *IEEE Open J. Ind. Appl.*, vol. 2, pp. 93–109, Apr. 2021.

[12] C. Yang, L. Huang, H. Xin, and P. Ju, "Placing grid-forming converters to enhance small signal stability of PLL-integrated power systems," *IEEE Trans. Power Syst.*, vol. 36, no. 4, pp. 3563–3573, Jul. 2021.

[13] N. Pogaku, M. Prodanovic, and T. C. Green, "Modeling, analysis and testing of autonomous operation of an inverter-based microgrid," *IEEE Trans. Power Electron.*, vol. 22, no. 2, pp. 613–625, Mar. 2007.

[14] H.-P. Beck and R. Hesse, "Virtual synchronous machine," in *Proc. 9th Int. Conf. Elect. Power Qual. Utilisation*, 2007, pp. 1–6.

[15] Q. Zhong and G. Weiss, "Synchronverters: Inverters that mimic synchronous generators," *IEEE Trans. Ind. Electron.*, vol. 58, no. 4, pp. 1259–1267, Apr. 2011.

[16] D. Pan, X. Wang, F. Liu, and R. Shi, "Transient stability of voltage-source converters with grid-forming control: A design-oriented study," *IEEE J. Emerg. Sel. Top. Power Electron.*, vol. 8, no. 2, pp. 1019–1033, Jun. 2020.

[17] P. C. Loh and D. G. Holmes, "Analysis of multiloop control strategies for LC/CL/LCL-filtered voltage-source and current-source inverters," *IEEE Trans. Ind. Appl.*, vol. 41, no. 2, pp. 644–654, Mar./Apr. 2005.

[18] T. Qoria, F. Gruson, F. Colas, X. Guillaud, M.-S. Debry, and T. Prevost, "Tuning of cascaded controllers for robust grid-forming voltage source converter," in *Proc. Power Syst. Comput. Conf.*, 2018, pp. 1–7.

[19] H. Xin, L. Huang, L. Zhang, Z. Wang, and J. Hu, "Synchronous instability mechanism of P-f droop-controlled voltage source converter caused by current saturation," *IEEE Trans. Power Syst.*, vol. 31, no. 6, pp. 5206–5207, Nov. 2016.

[20] J. Yu, Y. Qi, H. Deng, X. Liu, and Y. Tang, "Evaluating small-signal synchronization stability of grid-forming converter: A geometrical approach," *IEEE Trans. Ind. Electron.*, vol. 69, no. 9, pp. 9087–9088, Sep. 2022.

[21] M. Li et al., "Unified modeling and analysis of dynamic power coupling for grid-forming converters," *IEEE Trans. Power Electron.*, vol. 37, no. 2, pp. 2321–2337, Feb. 2022.

[22] T. Qoria, F. Gruson, F. Colas, X. Kestelyn, and X. Guillaud, "Analysis of the coupling between the outer and inner control loops of a grid-forming voltage source converter," in *Proc. 22nd Eur. Conf. Power Electron. Appl.*, 2020, pp. P.1–P.10.

[23] S. D'Arco, J. A. Suul, and O. B. Fosso, "Automatic tuning of cascaded controllers for power converters using eigenvalue parametric sensitivities," *IEEE Trans. Ind. Appl.*, vol. 51, no. 2, pp. 1743–1753, Mar./Apr. 2015.

[24] F. Cecati, M. Liserre, Y. Liao, X. Wang, and F. Blaabjerg, "Design oriented analysis of control loops interaction in power synchronization-based voltage source converter," in *Proc. IEEE Energy Convers. Congr. Expo.*, 2021, pp. 3282–3288.

[25] Y. Li, Y. Gu, Y. Zhu, A. Junyent-Ferré, X. Xiang, and T. C. Green, "Impedance circuit model of grid-forming inverter: Visualizing control algorithms as circuit elements," *IEEE Trans. Power Electron.*, vol. 36, no. 3, pp. 3377–3395, Mar. 2021.

[26] Y. Xia, M. Yu, X. Wang, and W. Wei, "Describing function method based power oscillation analysis of *LCL*-filtered single-stage PV generators connected to weak grid," *IEEE Trans. Power Electron.*, vol. 34, no. 9, pp. 8724–8738, Sep. 2019.

Jianing Liu (Student Member, IEEE) received the B.Eng. degree in electrical engineering and its automation from the Light Industry College, Liaoning University, Liaoning, China, and the Ph.D. degree in electrical engineering from the College of Electrical Engineering, Zhejiang University, Hangzhou, China, in 2017 and 2022, respectively.

His current research interests include modeling, control, and stability analysis of power systems with renewable energy.

Yanghong Xia (Member, IEEE) received the B.S. degree in automation from the College of Automation, Huazhong University of Science and Technology, Wuhan, China, and the Ph.D. degree in control theory and control engineering from the College of Electrical Engineering, Zhejiang University (ZJU), Hangzhou, China, in 2014 and 2019, respectively.

He was a Post-doctoral Research Fellow in the joint postdoctoral fellowship program between ZJU and the University of Cambridge, Cambridge, U.K, from 2019 and 2020. He is currently with the College of Electrical Engineering, Zhejiang University. His current research interests include hydrogen production, renewable energy sources, advanced control methods, stability analysis of power system, and hybrid ac/dc microgrid.

Wei Wei received the B.Eng. degree in automation, the M.Eng. degree in control theory and control engineering, and D.Eng. degree in power electronics and electronic drives from the College of Electrical Engineering, Zhejiang University, China, in 1983, 1986, and 1994, respectively.

He is currently a Professor with the College of Electrical Engineering, Zhejiang University. His current research interests include intelligent control, the development of novel technology of renewable energy and smart grid.

Qifan Feng received the B.S. degree in automation from the College of Electrical Engineering, Shandong University, Jinan, China, in 2021. He is currently working toward the Ph.D. degree in electrical engineering with the College of Electrical Engineering, Zhejiang University, Hangzhou, China.

His research interests include distributed photovoltaic power generation and power quality analysis and management.

Pengcheng Yang (Member, IEEE) received the B.S. degree from the College of Automation, Huazhong University of Science and Technology, Wuhan, China, in 2015, and the Ph.D. degree in electrical engineering from the College of Electrical Engineering, Zhejiang University, Hangzhou, China in 2020.

From 2020 to 2023, he was a Postdoctoral Researcher with Zhejiang University. His current research interests include modeling and control of microgrid and complex behavior of distributed generations.